Supplemental Material for Benchmark problems for anisotropic curvature-driven shrinkage: a multi-phase field model study

Martin Minar* and Nele Moelans
KU Leuven, Deptartment of Materials Engineering
(Dated: July 20, 2022)

S.I. MODEL PARAMETERS DETERMINATION - BEST PRACTICES

The best practices in parameters determination described in this section were implemented in MATLAB functions, which were published in dataset [1], distributed under GPLv3 license.

A. Polynomial expressions for determination of γ

Interface energy and width are non-analytic functions of the parameter γ (equations (6) and (7) in the main text). In models IWc and IWvG with non-uniform interface energy, γ varies in space and depends on physical input (local interface energy σ) and chosen interface width. Assuming that κ, m and σ are known, $g(\gamma)$ is computed using equation (6) and must be inverted in order to obtain γ. For numeric convenience, functions $g^2 \to 1/\gamma$ and $1/\gamma \to f_{0,c}$ were fitted by polynomials using the tabulated values from [2]. The same approach was taken in [3]. Note that in one of the following subsections an alternative algorithm for determination of parameters in IWc is proposed.
The values of $f_{0,c}(\gamma), g(\gamma)$ were tabulated and published in [2] in the range $0.52 \leq \gamma \leq 40$. However, the polynomials used in both [2, 3] did not describe the functions along the whole tabulated range. For inconvenient input, that resulted in a loss of control over the interface properties (even negative values of γ were obtained).
To improve the parameters determination, the functions $g^2 \to 1/\gamma$ and $1/\gamma \to f_{0,c}$ were fitted again so that all γ values from the interval $0.52 \leq \gamma \leq 40$ were reliably available. The new polynomials show good agreement along the given interval and their coefficients are listed in Table S.1.

TABLE S.1: Coefficients of the new polynomials used in the parameters determination algorithm (IWc and IWvG models). Based on fitting of the numeric values given in [2]. The polynomial of order N $p_N(x)$ is defined here together with its coefficients as $p_N(x) = \sum_{i=0}^{N} a_i x^{N-i}$. See text for details of use in the respective models.

	order	a_0	a_1	a_2	a_3	a_4	a_5	a_6
$g^2 \to \frac{1}{\gamma}$	6	-5.73008	18.8615	-23.0557	7.47952	8.33568	-8.01224	2.00013
$\frac{1}{\gamma} \to \sqrt{f_{0,c}}$	5	-0.072966	0.35784	-0.68325	0.63578	-0.48566	0.53703	
$g\sqrt{f_{0,c}} \to \frac{1}{\gamma}$	6	103.397	-165.393	105.3469	-44.55661	24.7348	-11.25718	1.999642

B. IWvG

This parameters determination algorithm [2] requires input of initializing interface energy σ_{init}, and width l_{init} which are assigned to interface with value $\gamma = 1.5$. There, the analytic relations between the model parameters are valid and the (constant) parameters κ, m can be computed:

$$\kappa = \frac{3}{4}\sigma_{init} l_{init} \quad , \quad m = 6\frac{\sigma_{init}}{l_{init}} \,. \tag{S.1}$$

These are then used in equation (6) with individual interface energies $\sigma_{i,j}$ to determine $g^2(\gamma_{i,j})$ and further $\gamma_{i,j}$ (using the first polynomial from Table S.1).

* martin.minar1132@gmail.com

However, because the said polynomial was only fitted in the interval $0.52 \leq \gamma \leq 40$ (values tabulated in [2]), it is important to choose the value of σ_{init} such, that none of the interface energies $\sigma_{i,j}$ should be described by $\gamma_{i,j}$ out of the interval. From equation (6) with substituted $\sqrt{\kappa m}$ from S.1 we show that the values do not leave the above interval when σ_{init} complies with the following two inequalities

$$\frac{\sigma_{max}}{g(40)}\sqrt{\frac{2}{9}} \leq \sigma_{init} \leq \frac{\sigma_{min}}{g(0.52)}\sqrt{\frac{2}{9}}\,, \tag{S.2}$$

where $\sigma_{min}, \sigma_{max}$ are minimal and maximal interface energy present in the system. Additionally, in order to fulfill these conditions, it must be satisfied that

$$\frac{\sigma_{min}}{\sigma_{max}} \geq \frac{g(0.52)}{g(40)} = \frac{0.1}{0.76} = 0.129\,, \tag{S.3}$$

which sets the maximal anisotropy in interface energy for which all $\gamma_{i,j}$s may be determined in IWvG based on the values tabulated in [2].
Control over the width of the narrowest interface (with user-defined width l_{min}) is obtained when the parameters are determined in two steps as follows:

1. values of κ, m are calculated from equations (S.1) using appropriate σ_{init} together with l_{min}
2. values of κ, m are recalculated from equations (S.1) with the same σ_{init} and interface width $l_{calib} = l_{min}\sqrt{8 f_{0,c}(\gamma_{min})}$, where γ_{min} corresponds to the lowest value of all the $\gamma_{i,j}$ obtained in the previous step, i.e. to the interface with the largest interface energy σ_{max}.

After the second step, the interface with maximal interface energy will have the width l_{min} and all the other interfaces will have it equal or larger.

The other interface widths can be expressed

$$l_{i,j} = \frac{\sigma_{i,j}}{m}\frac{1}{g(\gamma_{i,j})\sqrt{f_{0,c}}(\gamma_{i,j})} \tag{S.4}$$

C. IWc

The iterative parameters determining procedure assuring the constant interface width is described in [3]. The procedure requires initializing value of interface energy σ_{init}, which has decisive role for the parameters values. For inconvenient choice of σ_{init}, some of the parameters $\gamma_{i,j}$ may get out of range of applicability of the polynomials in Table S.1. Systematic investigation revealed that the value $\sigma_{init} = (\sigma_{max} + \sigma_{min})/2$ prevents occurrence of such effects for anisotropies $\sigma_{min}/\sigma_{max} \geq 0.03$.
Here we propose a simplified, yet equivalent single-step procedure. We assume constant interface width l and an initializing interface energy σ_{init}, for which $\gamma = 1.5$ and thus the analytic relations between the model parameters hold. As in the original iterative algorithm, the barrier height is computed

$$m = 6\frac{\sigma_{init}}{l}. \tag{S.5}$$

Then, the gradient energy coefficient $\kappa_{i,j}$ can be expressed from both equations (7) and (8), hence we can write

$$\kappa_{i,j} = f_{0,c}(\gamma_{i,j}) m l^2 = \sigma_{i,j} l \frac{\sqrt{f_{0,c}(\gamma_{i,j})}}{g(\gamma_{i,j})}\,, \tag{S.6}$$

from where we obtain

$$g(\gamma_{i,j})\sqrt{f_{0,c}(\gamma_{i,j})} = \frac{\sigma_{i,j}}{ml} = \frac{\sigma_{i,j}}{6\sigma_{init}}\,. \tag{S.7}$$

In the last equation, m was substituted from (S.5). We denote $G(\gamma_{i,j}) = g(\gamma_{i,j})\sqrt{f_{0,c}(\gamma_{i,j})}$. This function $\gamma \to G$ can be evaluated from the data tabulated in [2] and its inverse function $G \to \frac{1}{\gamma}$ was fitted by 6-th order polynomial producing the coefficients in the last row of Table S.1. Apparently, evaluation of this polynomial in points $\sigma_{i,j}/6\sigma_{init}$

produces the searched $1/\gamma_{i,j}$. The gradient energy coefficients are then best computed as in S.6, where m was substituted from S.5:

$$\kappa_{i,j} = 6 f_{0,c}(\gamma_{i,j}) \sigma_{init} l \,. \tag{S.8}$$

Here, the fitted polynomial $\frac{1}{\gamma} \to \sqrt{f_{0,c}}$ is used to obtain the values of $f_{0,c}(\gamma_{i,j})$.

Similarly like in IWcG model, there are conditions limiting suitable values of σ_{init}

$$\frac{\sigma_{max}}{6G(40)} \leq \sigma_{init} \leq \frac{\sigma_{min}}{6G(0.52)} \,, \tag{S.9}$$

where $G(0.52) \approx 0.0069, G(40) \approx 0.4065$. Also must be satisfied

$$\frac{\sigma_{min}}{\sigma_{max}} \geq \frac{G(0.52)}{G(40)} = 0.017 \,. \tag{S.10}$$

The main advantage of the proposed algorithm is that no iterations are needed for parameters determination. In the original algorithm the number of iteration steps is uncertain (tens of repetitions are not exceptional though) and sometimes the results may not converge due to reasons tedious to debug. Obtaining each parameter in a single step thus provides better control over the process and simplifies the implementation. Moreover, the permissible values of σ_{init} and the maximal anisotropy $\sigma_{min}/\sigma_{max}$ are clearly defined.

Also, it should be noted that when σ_{init} is chosen close to the upper limit in the inequality S.9, the determined $\gamma_{i,j}$s are rather closer to value 0.52 (corresponding to long-tailed interfaces). When σ_{init} is near the bottom limit, the values of γ_{max} are close to the value 40 and γ_{min} are much larger than in the previous case. Near the limiting anisotropy $\sigma_{min}/\sigma_{max} \approx 0.017$, the values always are $\gamma_{max} \approx 40$ and $\gamma_{min} \approx 0.52$. It is especially near the limits of admissible σ_{init}, where the original iterative parameters assignment strategy is not always reliable when compared to the proposed one.

D. IWvK

When $\gamma = const = 1.5$, the analytic relations between the model parameters hold (i.e. equations (8)-(10)). Then, the minimal interface width l_{min} is controlled when

$$m = 6 \frac{\sigma_{min}}{l_{min}} \tag{S.11}$$

and

$$\kappa_{i,j} = \frac{9}{2} \frac{\sigma_{i,j}^2}{m} \,. \tag{S.12}$$

Interface width of an interface i-j can then be computed as

$$l_{i,j} = 6 \frac{\sigma_{i,j}}{m} \,. \tag{S.13}$$

S.II. PROPERTIES OF THE USED ANISOTROPY FUNCTION

Let $f(\theta)$ be a smooth anisotropy function in 2D (see e.g. [4] for more details). The Wulff shape $\boldsymbol{w}$ in 2D is a curve minimizing the interface energy of a crystal with constant area. It can be parameterized by the interface normal angle θ, i.e. $\boldsymbol{w}(\theta) = [w_x(\theta), w_y(\theta)]^{\mathrm{T}}$, giving [4–6]

$$w_x(\theta) = R_W [f(\theta)\cos(\theta) - f'(\theta)\sin(\theta)] \tag{S.14}$$
$$w_y(\theta) = R_W [f(\theta)\sin(\theta) + f'(\theta)\cos(\theta)] \,, \tag{S.15}$$

where R_W is the radius of the Wulff shape (arbitrary). The radius of curvature $\varrho(\theta)$ of this Wulff shape is locally

$$\varrho(\theta) = R_W [f''(\theta) + f(\theta)] \,, \tag{S.16}$$

which may technically get negative for some θ. Because that does not have any geometric interpretation, the Wulff shape does not contain such oriented segments and the angles θ_m fulfilling $\varrho(\theta_m) \leq 0$ are called missing or forbidden. In the following, we assume the anisotropy function

$$f(\theta) = 1 + \delta \cos(n\theta) \tag{S.17}$$

with strength of anisotropy $0 \leq \delta < 1$ and n an order of symmetry (integer). The interface energy is $\sigma = \sigma_0 f(\theta)$. In this case, the missing angles occur for sufficiently strong anisotropy, i.e. when

$$\delta \geq \frac{1}{n^2 - 1}\,, \tag{S.18}$$

and span over an interval around every maximum of anisotorpy function $f(\theta)$. The stronger the anisotropy, the wider the interval of missing angles. Within $-\frac{\pi}{n} \geq \theta \leq \frac{\pi}{n}$, the border points of that interval are found by solving [6]

$$\frac{\mathrm{d}}{\mathrm{d}\theta}\frac{\cos(\theta)}{f(\theta)} = 0\,. \tag{S.19}$$

As the authors are unaware of analytic solution to this equation, it was solved numerically. The other (n-1) segments on the Wulff shape are periodic, hence all the missing angles can be obtained by rotation of the above one by multiples of $2\pi/n$.

The strong-anisotropy Wulff shape is not smooth, it contains corners (i.e. jumps in local normal orientation). When plotting such Wulff shape, the missing angles θ_m must be excluded from the θs parameterizing $\boldsymbol{w}(\theta)$, otherwise "ears" behind the corners are plotted as well.

Equation (S.18) can be used to define normalized strength of anisotropy $\Omega = \delta(n^2 - 1)$, which straightforwardly distinguishes between weak anisotropy $\Omega < 1$ (smooth Wulff shape) and strong anisotropy $\Omega \geq 1$ (the cornered one).

For a given radius R_W, the area of a Wulff shape A_W differs from the area of a circle $A = \pi R_W^2$ by the anisotropy-dependent factor $C_W(\Omega, n) = A_W/A$. For weak anisotropy $\Omega < 1$ there is an analytic expression

$$C_W = 1 - \frac{\Omega^2}{n^2 - 1}\,, \tag{S.20}$$

but there is none for strong anisotropy $\Omega > 1$. The factor $C_W(\Omega, n)$ was obtained numerically for $n = 4$ in the range $0 \leq \Omega \leq 7.5$ (the Wulff shape was plotted, its area numerically computed and divided by πR^2). There, the Ω-dependence was fitted very well by a polynomial of 4-th order $C_W(\Omega, 4) = \sum_{i=0}^{4} a_i \Omega^{N-i}$ with $a_0 = -0.00032, a_1 = 0.00639, a_2 = -0.04219, a_3 = 0.00034, a_4 = 1.00000$.

S.III. SHRINKAGE RATE OF A WULFF SHAPE

The normal velocity of anisotropic curvature-driven interface in 2D is [7]

$$v_n(\theta, t) = -\frac{\mu}{\varrho(\theta, t)}\sigma_0[f''(\theta) + f(\theta)] \tag{S.21}$$

where μ is the interface mobility and $\sigma_0[f''(\theta) + f(\theta)]$ is interface stiffness. When it is the Wulff shape shrinking, the radius of curvature $\varrho(\theta, t)$ can be expressed as in equation (S.16) and the inclination-dependent part of the interface stiffness is cancelled out. The normal velocity is then constant along the perimeter

$$v_n(t) = -\frac{\mu\sigma_0}{R_W(t)}\,. \tag{S.22}$$

The sign is such that the interface moves towards the center of curvature.

Because the area of a Wulff shape is $A_W = \pi R_W^2 C_W(\Omega, n)$, the shrinkage rate of a Wulff shape is

$$\begin{aligned}\frac{\mathrm{d}A_W}{\mathrm{d}t} &= \frac{\mathrm{d}}{\mathrm{d}t}[\pi R_W^2(t) C_W(\Omega, n)] \\ &= 2\pi C_W(\Omega, n) R_W(t)\frac{\mathrm{d}R_W}{\mathrm{d}t}\,.\end{aligned} \tag{S.23}$$

TABLE S.2: Parameters from equation (S.27) describing anisotropic dependence of the Courant number C in simulations with inclination-dependent interface energy and strong anisotropy $\Omega > 1$.

	IWc	IWvG	IWvK
a	1.38	1.43	0.98
b	1.95	1.91	2.35

Because the normal velocity is constant along the perimeter, the point R_{min} from equation (37) moves also by $v_n(t)$. Importantly, the normal of interface in R_{min} is aligned with the radial direction of the polar coordinates, hence we can write $v_n = \mathrm{d}R_{min}/\mathrm{d}t$. From equation (37) then must be

$$\frac{\mathrm{d}R_W}{\mathrm{d}t} = \frac{1}{1-\delta}\frac{\mathrm{d}R_{min}}{\mathrm{d}t} = \frac{1}{1-\delta}v_n(t)\,, \tag{S.24}$$

which together with S.22 implies in S.23

$$\frac{\mathrm{d}A_W}{\mathrm{d}t} = 2\pi\mu\sigma_0\frac{C_W(\Omega,n)}{1-\delta} \tag{S.25}$$

Taylor and Cahn [8] proved that the shrinkage rate for the equilibrium shape must be a constant, which is met by the final expression.

S.IV. ADDITIONAL REMARKS ON NUMERIC IMPLEMENTATION

In finite difference method, the ratio of the time step to the grid spacing determines the numeric stability of the simulation. Specifically, the so-called Courant number C must be $0 < C < 0.5$, where in this model

$$C = \min[\kappa(\boldsymbol{r})L]\Delta t/(\Delta x)^2\,. \tag{S.26}$$

In practice, the time step was computed using equation (S.26) assuming the value of $C \leq 0.3$. For stronger anisotropies C had to be reduced farther. When $0.129 \leq \sigma_{min}/\sigma_{max} \leq 0.2$, the value $C = 0.12$ was used, when $0.2 < \sigma_{min}/\sigma_{max} \leq 0.3$, $C = 0.17$ and for $\sigma_{min}/\sigma_{max} > 0.3$ the used Courant number was $C = 0.3$. The latter value of Courant number was also applied in simulations with inclination-dependent interface energy and smooth Wulff shapes ($\Omega \leq 1$). For cornered Wulff shapes ($\Omega > 1$), the following dependence was obtained from visual inspection of the interface normal inclination field $\theta(\boldsymbol{r})$ defined in equation (18) ($\theta(\boldsymbol{r})$ was sensitive to the numeric instabilities) during the simulation

$$C(\Omega) = \frac{1}{a\Omega + b}\,. \tag{S.27}$$

The Table S.2 contains the values of a, b in the respective model modifications.

The following 9-point stencil was used for computation of the laplacian in grid point (k, l)

$$\begin{aligned}(\nabla^2\eta)_{k,l} = \frac{1}{6h^2}[&4(\eta_{k-1,l} + \eta_{k+1,l}\eta_{k,l-1} + \eta_{k,l+1}) \\ &+ \eta_{k+1,l+1} + \eta_{k-1,l-1} + \eta_{k-1,l+1} + \eta_{k+1,l-1} \\ &- 20\eta_{k,l}]\,.\end{aligned} \tag{S.28}$$

When the interface energy is inclination-dependent, it can be seen in equations (23), (24) of the main text that some driving force terms are proportional to $1/|\nabla\eta_i - \nabla\eta_j|$. In fact, some are even proportional to $1/|\nabla\eta_i - \nabla\eta_j|^3$ when worked out analytically. Far enough from the interface, the magnitude $|\nabla\eta_i - \nabla\eta_j|$ inevitably gets smaller than the numeric resolution, which causes severe numeric instabilities due to locally very large driving forces. For this reason, all the driving force terms from equation (21) were only computed in a region close enough to the interface. Two such regions $\Gamma_{out}, \Gamma_{inn}$ (outer and inner) were selected based on local value of $|\nabla\eta_i - \nabla\eta_j|$ (see Figure S.1). The region Γ_{inn} was a subset of Γ_{out}. The interface inclination field $\theta_{i,j}$ was computed in Γ_{out}, where $|\nabla\eta_i - \nabla\eta_j|^3(\Delta x)^3 > C_{out}^3$ and the driving force terms $\nabla \cdot \partial f/\partial(\nabla\eta_p)$ were computed in region Γ_{inn} where $|\nabla\eta_i - \nabla\eta_j|^3(\Delta x)^3 > C_{inn}^3$. The constants $C_{out} = 10^{-6}$ and $C_{inn} = 0.005$ have the meaning of minimal local change in value of phase field which is acceptable to the respective near-interface region (this is exactly true for $\gamma = 1.5$ and approximate otherwise). Note, that the driving force from homogeneous free energy density (i.e. $\partial f/\partial\eta_p$) and the laplacian term $\kappa(\boldsymbol{r})\nabla^2\eta_p$ were computed and applied in the whole simulation domain.

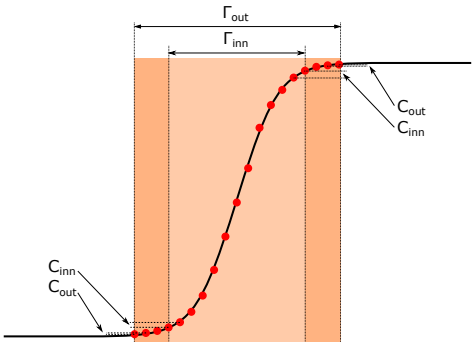

FIG. S.1: Illustration of the near-interface regions $\Gamma_{out}, \Gamma_{inn}$, defined by absolute values of difference in phase fields between neighbouring points.

In the Wulff shape simulations, the accuracy of match to the analytical shape with IWvG phase field contour turned out to be sensitive to alignment of the shape within the numerical grid. For strong anisotorpies $\Omega > 1$, when the corner laid exactly on some grid line, the IWvG contours were slightly deformed, making the model perform seemingly worse than IWc and IWvK (which were not affected by this). This problem was solved by shifting the center of the initial shape by half a pixel in both x and y direction. No corner than laid on any grid line and that solved the problem. Rotating the Wulff shape relative to the grid had similar effect. All the results in the main text were simulated with the shifted initial shape. This is not likely to play significant role in grain growth simulations as the corner motion along grid line is very unlikely with arbitrary grain structure and local grain orientation.

[1] M. Minar, Benchmarking of different strategies to include anisotropy in a curvature-driven multi-phase-field model, Mendeley Data, v2 10.17632/5wrv3ky9pp.2 (2022).
[2] H. Ravash, J. Vleugels, and N. Moelans, Three-dimensional phase-field simulation of microstructural evolution in three-phase materials with different interfacial energies and different diffusivities, Journal of Materials Science **52**, 13852 (2017).
[3] N. Moelans, B. Blanpain, and P. Wollants, Quantitative analysis of grain boundary properties in a generalized phase field model for grain growth in anisotropic systems, Physical Review B - Condensed Matter and Materials Physics **78**, 10.1103/PhysRevB.78.024113 (2008).
[4] R. Kobayashi and Y. Giga, On anisotropy and curvature effects for growing Crystals, Japan Journal of Industrial and Applied Mathematics **18**, 207 (2001).
[5] W. K. Burton, N. Cabrera, and F. C. Frank, The Growth of Crystals and the Equilibrium Structure of their Surfaces, Philosophical Transactions of the Royal Society A: Mathematical, Physical and Engineering Sciences **243**, 299 (1951).
[6] J. Eggleston, G. McFadden, and P. Voorhees, A phase-field model for highly anisotropic interfacial energy, Physica D: Nonlinear Phenomena **150**, 91 (2001).
[7] F. Abdeljawad, S. M. Foiles, A. P. Moore, A. R. Hinkle, C. M. Barr, N. M. Heckman, K. Hattar, and B. L. Boyce, The role of the interface stiffness tensor on grain boundary dynamics, Acta Materialia **158**, 440 (2018).
[8] J. E. Taylor and J. W. Cahn, Diffuse interfaces with sharp corners and facets: Phase field models with strongly anisotropic surfaces, Physica D: Nonlinear Phenomena **112**, 381 (1998).